Recovery and normalization of triple coincidences in PET

Eduardo Lage[a)] and Vicente Parot
Madrid-MIT M+Visión Consortium, Massachusetts Institute of Technology, Cambridge, Massachusetts 02139

Stephen C. Moore and Arkadiusz Sitek
Division of Nuclear Medicine, Department of Radiology, Harvard Medical School and Brigham and Women's Hospital, Boston, Massachusetts 02115

Jose M. Udías
Grupo de Física Nuclear, Departamento de Física Atómica Molecular y Nuclear, Universidad Complutense de Madrid, CEI Moncloa, Madrid 28040, Spain

Shivang R. Dave
Madrid-MIT M+Visión Consortium, Massachusetts Institute of Technology, Cambridge, Massachusetts 02139

Mi-Ae Park
Division of Nuclear Medicine, Department of Radiology, Harvard Medical School and Brigham and Women's Hospital, Boston, Massachusetts 02115

Juan J. Vaquero
Departamento de Ingeniería Biomédica e Ingeniería Aeroespacial, Universidad Carlos III de Madrid, Leganés 28911, Spain

Joaquin L. Herraiz
Madrid-MIT M+Visión Consortium, Massachusetts Institute of Technology, Cambridge, Massachusetts 02139

Purpose: Triple coincidences in positron emission tomography (PET) are events in which three γ-rays are detected simultaneously. These events, though potentially useful for enhancing the sensitivity of PET scanners, are discarded or processed without special consideration in current systems, because there is not a clear criterion for assigning them to a unique line-of-response (LOR). Methods proposed for recovering such events usually rely on the use of highly specialized detection systems, hampering general adoption, and/or are based on Compton-scatter kinematics and, consequently, are limited in accuracy by the energy resolution of standard PET detectors. In this work, the authors propose a simple and general solution for recovering triple coincidences, which does not require specialized detectors or additional energy resolution requirements.

Methods: To recover triple coincidences, the authors' method distributes such events among their possible LORs using the relative proportions of double coincidences in these LORs. The authors show analytically that this assignment scheme represents the maximum-likelihood solution for the triple-coincidence distribution problem. The PET component of a preclinical PET/CT scanner was adapted to enable the acquisition and processing of triple coincidences. Since the efficiencies for detecting double and triple events were found to be different throughout the scanner field-of-view, a normalization procedure specific for triple coincidences was also developed. The effect of including triple coincidences using their method was compared against the cases of equally weighting the triples among their possible LORs and discarding all the triple events. The authors used as figures of merit for this comparison sensitivity, noise-equivalent count (NEC) rates and image quality calculated as described in the NEMA NU-4 protocol for the assessment of preclinical PET scanners.

Results: The addition of triple-coincidence events with the authors' method increased peak NEC rates of the scanner by 26.6% and 32% for mouse- and rat-sized objects, respectively. This increase in NEC-rate performance was also reflected in the image-quality metrics. Images reconstructed using double and triple coincidences recovered using their method had better signal-to-noise ratio than those obtained using only double coincidences, while preserving spatial resolution and contrast. Distribution of triple coincidences using an equal-weighting scheme increased apparent system sensitivity but degraded image quality. The performance boost provided by the inclusion of triple coincidences using their method allowed to reduce the acquisition time of standard imaging procedures by up to ~25%.

Conclusions: Recovering triple coincidences with the proposed method can effectively increase the sensitivity of current clinical and preclinical PET systems without compromising other

1. INTRODUCTION

High sensitivity is a critical performance parameter of positron emission tomography (PET) scanners required for obtaining images with acceptable values of signal-to-noise ratio (SNR). This is especially relevant to reduce scan times in long procedures (e.g., a whole body scan) or when performing dynamic or gated studies. The sensitivity of a PET scanner is mainly determined by the intrinsic efficiency of the detection system (fraction of incident photons detected) and the solid angle coverage of the imaged object or patient. Unfortunately, increasing the sensitivity by using better detector materials[1] or extending the axial field-of-view (FOV) by adding more detectors[2] significantly increases the cost of PET scanners.

A different approach suggested for improving the sensitivity of PET consists of using triple coincidences which are events in which three γ-rays are detected simultaneously by the scanner (Fig. 1). Most commonly, these interactions define at least one valid line-of-response (LOR_{1-2} in both examples), and therefore, they contain useful information that can be used to reconstruct images with better quality. Nevertheless, these coincidences are often discarded or processed without special consideration by clinical and preclinical scanners since there is not a clear criterion to establish which LOR of those defined by the triple coincidence [LOR_{1-2}, LOR_{1-3} and LOR_{2-3} in (Fig. 1)] is the correct one along which the decay occurred. It is important to note that triple coincidences occur normally and with high frequency in any PET acquisition, even when using standard pure positron emitter radionuclides like ^{18}F, ^{11}C, or ^{13}N. There are several sources of triple coincidences, for example, interdetector scattered (IDS) events [Fig. 1 (left)] are triple interactions in which one of the photons coming from a positron annihilation deposits all its energy in one detector

and the other deposits its energy among at least two detectors. Although the number of these IDS events relative to standard double coincidences depends on the scanner configuration (e.g., on the crystal's stopping power), in most current commercial systems (which are based on rings of block detectors[3–6]) the ratio between IDS and double coincidences is on the order of 20%.[7,8] In some special preclinical scanners with single-crystal read-out like the MADPET-II (Ref. 9) or the LabPET,[10,11] much higher IDS to double coincidence ratios have been reported [35% (Ref. 12) and 57%,[13] respectively] due to the possibility of detecting intercrystal scattered events. Random triple events (Rn_T) are another type of triple coincidences [Fig. 1 (right)] in which two γ-rays from one annihilation are detected simultaneously with another γ-ray from a different annihilation. Unlike IDS events, the relative number of Rn_T events increases with the activity concentration within the FOV of the scanner, as is the case with standard random double events. Moreover, when positron-gamma emitters like ^{124}I, ^{76}Br, ^{86}Y, or ^{94m}Tc are used in a PET scanner,[14] the additional prompt γ-rays emitted with positrons also generate triple and higher-order coincidence events[8] that can be recovered to enhance the photon sensitivity.[15] Finally, there are other processes which can also yield triple coincidences, like random triple events caused by three different decays, or positron annihilations generating three γ-rays via the formation of orthopositronium.[16] These events do not provide information about the LORs in which a decay occur, but as they are typically one or two orders of magnitude less frequent[8,17] than the aforementioned triple coincidences, we did not consider them in this work.

To the best of our knowledge, most commercial PET scanners simply ignore triple and higher-order coincidences and process the data to find photon pairs within predetermined time and energy windows. If this is the case, for IDS events, the scanner will record a double coincidence only if one of the IDS photons [2 or 3 in (Fig. 1)] deposits energy above a minimum threshold (e.g., 400 keV for a 400–700 keV energy window). This implies that the scanner will be discarding potentially useful information (IDS events in which both photons deposit energies under the lower energy threshold, e.g., 300 keV each) and that incorrect LORs are added to the dataset, i.e., the photon depositing the higher energy in an IDS event may or may not define the right LOR. For Rn_T events, there are three photons within the scanner energy window, so if triple interactions are not taken into account, then the three photons can be included as a set of double coincidences. For example, some clinical scanners[18] add this type of triple coincidences as one or two LORs when 1-pair or 2-pairs of photons are within the narrow-coincidence window of the scanner, respectively, and reject triples when all the singles are within this coincidence window (three valid LORs).
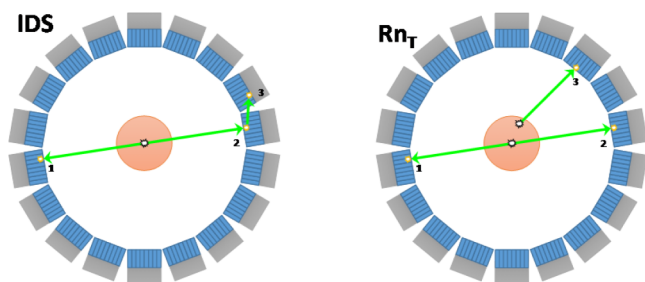

FIG. 1. Most common triple-coincidence events. (Left) Interdetector scatter event, IDS: one of the photons coming from the annihilation event interacts by photoelectric effect in one detector (1) and the other undergoes Compton scatter in other detector (2) and then photoelectric interaction in a neighboring detector (3). (Right) Random triple event, Rn_T: two photons coming from the same annihilation (1–2) are detected simultaneously with a photon from a different annihilation (3).

Methods for assigning IDS events to LORs have been previously suggested, including choosing the first interaction point based on the energy of the detected photons[7,19] or algorithms based on the kinematics of Compton scatter.[12,20] Since these methods are intrinsically limited by the energy resolution of detectors, other authors have investigated using all possible LORs defined by the triple event in the reconstruction by distributing them using the same weighting factors for all the possible LORs (e.g., 0.5/0.5 for a triple coincidence with two valid LORs). Overall, differences in performance among all of these methods have been found to be small,[12] and although apparent scanner sensitivity is increased, improvements in image quality arising from the addition of triple coincidences have not been convincingly demonstrated. In fact, the only work using real data from a scanner[13] found that adding IDS events using some of the aforementioned algorithms resulted in worse image quality than that achieved using only double coincidences (e.g., contrast-to-noise ratio was decreased between 7% and 10% and recovery coefficients between 9% and 14% with the best performing method).

Other approaches to recover multiple coincidences have been reported in nonstandard PET systems capable of recording the 3D coordinates of individual photon interactions.[21–24] In some of these studies,[21–23] the complete interaction sequence for each annihilation photon of IDS or intercrystal scattered events is delineated in order to select the earliest interactions and, thus, the points defining the LOR containing the original decay. In general, a Bayesian estimator based on Compton kinematics is used in an iterative reconstruction algorithm to ensure that all the interactions within each sequence are consistent with the entire dataset. Unlike the earlier studies, triple-coincidences and higher-order events were taken into consideration because the nonstandard design of these scanners means that IDS events are a significant fraction of the total events.[21,23] In another recent work,[24] the possibility of encoding into the system matrix on-the-fly calculated probabilities for the LORs defined by triple interactions was also investigated. Although the inclusion of IDS coincidences using these methodologies produced PET images with better image quality and spatial resolution comparable to those obtained using only double coincidences, the requirement of using a highly specialized detection system hampers general adoption of those approaches. Furthermore, the use of iterative reconstruction algorithms with such 3D detection systems and/or on-the-fly calculations of the elements of a system matrix requires a significant computational load[24] even when implemented on fast graphic processing units.[21]

In this work, we present a general methodology for assigning triple coincidences to LORs that can be used in both block- and specialized-detector-based scanners and has a negligible computational cost. This approach consists of using the standard PET double-coincidence dataset as a reference to assign probabilities to each of the possible LORs defined in a triple coincidence. The effect of including triple coincidences using this approach was compared in terms of sensitivity, noise-equivalent count (NEC) rates, and image quality with discarding all multiple events (e.g., using only double coincidences) and equally weighting the LORs in triple coincidences. While weighting the LORs equally is not a gold standard, we chose this algorithm to compare with our method because it represents the current state-of-the-art. All the experiments were performed using the PET component of a commercially available small-animal PET/CT scanner which was modified to enable the acquisition and processing of triple coincidences.

2. MATERIAL AND METHODS

2.A. Scanner

The PET component of the small-animal PET/CT scanner Argus/CT, manufactured by Sedecal S.A. (formerly eXplore Vista/CT commercialized by General Electric Healthcare), was used in this work. This scanner (hereafter called "Argus") consists of two rings of small-sized block detectors with depth-of-interaction (DOI) capability.[6,25] The detector modules have crystal arrays that contain two layers of 13×13 individual elements; the front-layer detectors are LYSO ($1.45 \times 1.45 \times 7$-mm deep) and the back-layer detectors are GSO ($1.45 \times 1.45 \times 8$-mm deep). Crystal arrays are optically glued at the GSO end to a position-sensitive photomultiplier tube (PS-PMT) with a 22×22 mm^2 active area (Hamamatsu R8520-00-C12).[26] Each ring is comprised of 18 of these modules, and each module is in coincidence with 14 opposing modules (7 in its own ring and 7 in the other ring). This configuration provides a transaxial FOV of 67 mm and an axial FOV of 48 mm.

During the scans, the acquisition electronics of the Argus send data packets to a control computer with information from single photons detected within a coarse-coincidence timing window (± 10 ns) and a coarse energy window (90 to 750 keV). The computer processes these packets in real-time to find valid double coincidences. To be classified as a valid coincidence, and consequently be recorded, each photon has to be detected within a user-specified energy window (100–700 keV, 250–700 keV, or 400–700 keV) and within a predefined narrow-coincidence time window (5 ns for LYSO-LYSO, 10 ns for GSO-GSO, and 7 ns for LYSO-GSO). The average timing resolution of this scanner was reported to be 1.3 ns full-width at half-maximum (FWHM) and the energy resolution for 511-keV photons averaged over all 6084 crystals was determined to be 26% ± 3.1% in the LYSO layer and 33% ± 4.8% in the GSO layer (mean ± SD).[25]

To enable the Argus scanner to detect and sort triple coincidences, we slightly tuned the hardware energy window to accept single photons in a 50 to 800 keV range. In addition, we rewrote the acquisition software to store optimized list-mode files containing all the information about single events detected (within the coarse-coincidence time window) during the acquisition; this information included the position of interaction, the energy, the crystal layer, and the timestamp (coarse + narrow). Another program was developed to analyze the list-mode files offline and group the single events into standard double coincidences, IDS events, or Rn$_T$ events using the following criteria.

- Double coincidences were identified when two single events were detected in opposite block detectors within the narrow-coincidence timing window of the scanner,

and furthermore, both events deposited energy between 400 and 700 keV.

- IDS events were identified as three events detected in three different block detectors within the narrow-coincidence timing window, with one event depositing energy between 400 and 700 keV and the remaining two events deposited a combined energy between 400 and 700 keV [Fig. 1 (left)].

- Rn_T events were identified as three photons detected in three different block detectors within the narrow-coincidence time window and each of them independently depositing energy between 400 and 700 keV [Fig. 1 (right)].

In this study, we restricted the data acceptance to triple coincidences because those represented the largest fraction of multiple coincidences in this system, as described in the Sec. 3. Finally, if a triple event did not meet the criteria for being classified as an IDS or a Rn_T event, but it had two valid photons (within both the time and energy windows), then those two photons were classified as a double coincidence.

2.B. Proportional method for recovering triple coincidences

To effectively use triple coincidences, it is logical to consider that a recovery method needs to select—among the possible LORs defined by the triple interaction [i.e., 1–2, 1–3, or 2–3 in (Fig. 1)]—the one along which the positron annihilation took place. Note that most of the time, one of the three possible LORs can be immediately discarded [2–3 in the example of (Fig. 1)], as it lies outside the FOV of the scanner. However, our method does not try to choose the correct LOR in each triple. Instead, it assumes that the distribution of the LORs defined by each triple interaction is given by the double-coincidence dataset and simply distributes the triple events among their possible LORs using the same distribution that was measured for double coincidences along these LORs,

$$LOR_{1-2} = D_{1-2} + \left(\frac{D_{1-2}}{D_{1-2} + D_{1-3}}\right)T,$$

$$LOR_{1-3} = D_{1-3} + \left(\frac{D_{1-3}}{D_{1-2} + D_{1-3}}\right)T. \tag{1}$$

To understand in an intuitive manner how and why this algorithm (hereafter referred to as the "proportional method") works, let us assume a simple PET scanner with only three detectors (Fig. 2). This assumption can be generalized to any PET scanner assuming statistical conditional independence of the detections on different LORs (a typical assumption in nuclear imaging). In this system, there are only two possible LORs (LOR_{1-2} and LOR_{1-3}), and triple coincidences must necessarily involve the three detectors. If we denote by D_{1-2} and D_{1-3} the number of double coincidences detected along LOR_{1-2} and LOR_{1-3}, respectively, and by T the number of
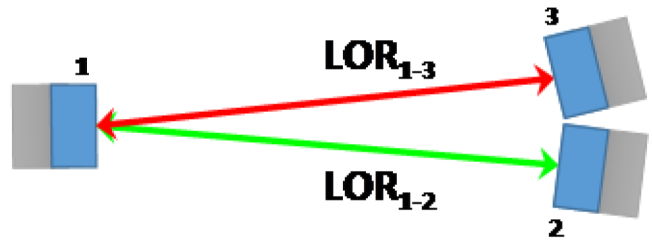

FIG. 2. Example PET scanner with only two possible LORs.

triple coincidences detected during the same acquisition (originating from a disintegration along either of these two LORs), our method will determine the mean of the number of counts along LOR_{1-2} and LOR_{1-3} (detected as double or triple) according to Eq. (1). We show below that under certain reasonable assumptions, the Eq. (1) is the maximum-likelihood (ML) estimate for the mean number of counts along LOR_{1-2} and LOR_{1-3}.

Let Y be a 3×1 random vector, containing the three aforementioned measurements of double and triple coincidences [$Y = (D_{1-2}; D_{1-3}; T)$]. We assume that Y is Poisson distributed with mean vector $Y^* = MX$, where M is a 3×2 linear coefficient matrix, whose elements represent the probability that a count emitted along any of the two LORs is detected by the camera either as D_{1-2}, D_{1-3}, or T. The X is a 2×1 vector containing the mean number of disintegrations along the LORs [$X = (LOR_{1-2}; LOR_{1-3})$]. For the sake of clarity, let us assume that the sensitivity of all detectors is the same and equals to 1. That is, if a decay occurs along one of the LORs, it will be detected with certainty (either as a double or a triple). We also assume that the probability of detecting any disintegration along LOR_{1-2} or LOR_{1-3} as a triple coincidence is the same, and equal to α, which leads to a matrix M = [[$1-\alpha$ 0]; [0 $1-\alpha$]; [α α]]. To find the ML estimate of X, we write the Poisson log-likelihood function for measurement Y, and omitting constant terms, we arrive to

$$L(Y^*|Y) = \sum_{i=1}^{n} (Y_i \log Y_i^* - Y_i^*),$$

where Y^* is [$(1 - \alpha)LOR_{1-2}$; $(1 - \alpha)LOR_{1-3}$; $\alpha(LOR_{1-2} + LOR_{1-3})$] and Y is our measurement [$Y = (D_{1-2}; D_{1-3}; T)$]. Then, the Poisson log–likelihood is given by Eq. (2) [note that the dependence on α's is factored in constant terms (not shown)],

$$L(Y^*|Y) = D_{1-2}\log(LOR_{1-2}) + D_{1-3}\log(LOR_{1-3})$$
$$+ T\log(LOR_{1-2} + LOR_{1-3}) - LOR_{1-2} - LOR_{1-3}. \tag{2}$$

Solving [Eq. (2)] for $dL/dLOR_{1-2} = 0$ and $dL/dLOR_{1-3} = 0$ to find the global maximum, we obtain that

$$\frac{D_{1-2}}{LOR_{1-2}} + \frac{T}{LOR_{1-2} + LOR_{1-3}} - 1 = 0,$$

$$\frac{D_{1-3}}{LOR_{1-3}} + \frac{T}{LOR_{1-2} + LOR_{1-3}} - 1 = 0.$$

And thus,

$$\text{LOR}_{1-2} = D_{1-2} + \frac{D_{1-2}}{D_{1-2} + D_{1-3}} T,$$

$$\text{LOR}_{1-3} = D_{1-3} + \frac{D_{1-3}}{D_{1-2} + D_{1-3}} T.$$

Using a more general notation, and since in a real scanner [i.e., a scanner with a full ring of detectors like the one shown in (Fig. 1)], there are LORs that have contributions from several triple coincidences (the same LOR can be defined by different triple combinations), the proposed method can be written using the following equation [Eq. (3)]:

$$\text{LOR}_{i-j} = D_{i-j} + \sum_{k}^{n} \left(\frac{D_{i-j}}{D_{i-j} + D_{i-k} + D_{j-k}} \right) T_{i-j-k}, \qquad (3)$$

where LOR_{i-j} represents the final number of counts coming either from double or triple coincidences along the LOR connecting the interaction points $i - j$, and D_{i-j}, D_{i-k} and D_{j-k} are the number of double coincidences detected between interaction points $i - j$, $i - k$, and $j - k$, respectively. T_{i-j-k} is the number of times a triple event involving interaction points $i - j - k$ was detected, and n is the number of triple coincidences that contribute to LOR_{i-j} As mentioned before, for each possible k value, there is a line-of-response that is outside of the FOV which should not be taken into account (either $D_{j-k} = 0$ or $D_{i-k} = 0$ for all k). Note also that for a practical implementation of this method, D_{i-j}, D_{i-k}, and D_{j-k} in Eq. (3) should ideally be the number of double coincidences along lines $i - j$, $i - k$, and $j - k$, respectively, after correction for efficiency (normalization) of each detector pair.

2.C. Normalization of triple coincidences and image reconstruction procedure

The correction for variations in detection efficiency of each LOR or sinogram bin in a scanner is known as "normalization" and has been thoroughly studied for PET imaging,[27,28] since inaccurate correction of these factors leads to artifacts that affect the quality of reconstructed images. In most previous studies,[12,13,21–23] no special considerations were made for the normalization of IDS or Rn_T coincidences, even though there is no reason to assume that the sensitivity of the scanner for such events should be similar to the sensitivity for double coincidences. In fact, in the mathematical demonstration shown

in Sec. 2.B, we also made this assumption to simplify the example.

To clarify this issue, we assumed that sensitivity and thus the normalization corrections for double, IDS, and Rn_T events are all different, and consequently, a specific normalization for each type of event is required. To evaluate this hypothesis, we acquired calibration data consisting of double and triple coincidences using a ^{68}Ge ring source for a 72-h acquisition time. Triple coincidences were separated into IDS and Rn_T events using the aforementioned energy and timing criteria. The double coincidences (400–700 keV) were stored in a sinogram [D terms in Eq. (3)], and the inverse of this sinogram was used as a multiplicative normalization correction for this type of events. To generate the normalization corrections for IDS and Rn_T coincidences, we used the triple-coincidence term of [Eq. (3)] assuming that all the lines defined by each triple had the same probability [0.5/0.5 since for each LOR_{i-j} either $D_{i-j} = D_{i-k}$ with $D_{j-k} = 0$ or $D_{i-j} = D_{j-k}$ with $D_{i-k} = 0$]. This distribution must be true when using a centered calibration ring source uniformly covering the FOV of the scanner. Note that this is equivalent to using in Eq. (3) the double-coincidence dataset after applying a normalization correction because, since the normalization is obtained from the same data to be corrected, the normalized data would be a sinogram containing a constant value in all the bins. During this process, the LOR distribution obtained for IDS and Rn_T events was stored in separated sinograms and, as was the case for double coincidences, the inverse of each of those sinograms was used as a multiplicative normalization correction for the corresponding type of event.

The flowchart in Fig. 3 illustrates how the proposed method for recovery and normalization of triple coincidences can be incorporated in a simple analytic reconstruction algorithm such as filtered backprojection (FBP). In the first step, raw data from the scanner are classified into double, IDS, and Rn_T events. Before using the doubles dataset in the recovery method, we apply to these data the corresponding normalization correction. Since in the proposed method the doubles dataset (stored into a LOR histogram or sinogram) is used as a reference to sort triple coincidences, the better the quality of this reference, the better the algorithm is expected to perform; therefore, additional standard corrections, e.g., for random or scattered events and attenuation, may also be applied at this point. After applying the proposed recovery method, we obtain
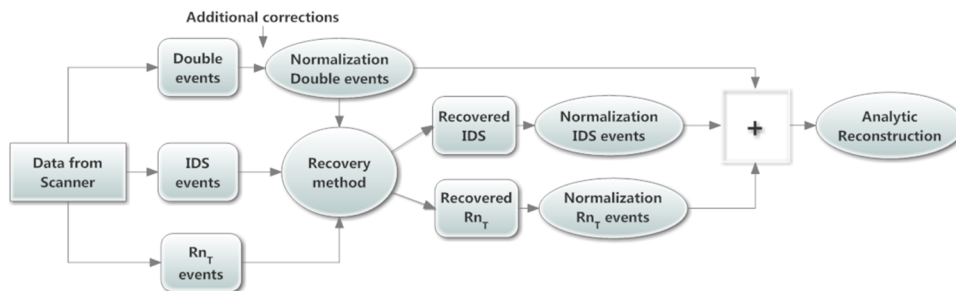

FIG. 3.   Example of implementation of the proposed recovery method in an analytic reconstruction framework: different types of triple events are recovered using the proposed method and a normalized doubles dataset. Recovered triple events are then normalized using matched normalization corrections for IDS and Rn_T coincidences. Normalized datasets (LOR histograms or sinograms, for example) are then added and reconstructed using an analytic reconstruction algorithm.

histograms or sinograms containing either recovered IDS or Rn_T events. These datasets are then normalized (by multiplying each dataset by their specific normalization corrections) and added to the already normalized double-event dataset before proceeding with the image reconstruction. The whole procedure is summarized by Eq. (4) in which we assume that D_{i-j}, D_{i-k}, and D_{j-k} are the number of double coincidences detected along the corresponding LORs after all the aforementioned corrections and α_{i-j}, β_{i-j} are normalization factors calculated as previously described for each specific type of triple coincidence (IDS and Rn_T, respectively) along LOR_{i-j},

$$LOR_{i-j} = D_{i-j} + \left[\sum_k^n \left(\frac{D_{i-j}}{D_{i-j} + D_{i-k} + D_{j-k}} \right) IDS_{i-j-k} \right] \alpha_{i-j}$$
$$+ \left[\sum_k^n \left(\frac{D_{i-j}}{D_{i-j} + D_{i-k} + D_{j-k}} \right) Rn_{T i-j-k} \right] \beta_{i-j}.$$
$$(4)$$

2.D. Performance evaluation

The effect on the performance of the scanner obtained by the inclusion of triple coincidences was measured in terms of absolute sensitivity, NEC rates for mouse- and rat-sized objects, and image quality. All these measurements were based on the NEMA NU-4 standard for the assessment of small-animal positron emission tomographs.[29]

In all cases, images containing double and double plus recovered triple coincidences were obtained following the method depicted in Fig. 3. Three-dimensional sinograms containing double or triple coincidences were rebinned into 61 sinograms with 175 radial × 128 angular bins using single-slice rebinning (SSRB) with a maximum ring difference of 7. After sensitivity correction, the resulting sinograms were added and reconstructed using 2D-FBP with a ramp filter into a 3D image volume with a voxel size of $0.39 \times 0.39 \times 0.78$ mm³. We preferred to use SSRB + FBP rather than an iterative algorithm for image reconstruction because it is a standard method which is available in any PET scanner and allows extrapolation of the results of this work to other systems. Additionally, while image SNR can be predicted by the NEC rate when using FBP reconstruction, studies suggest that this is not true when using 3D iterative reconstruction, particularly for those applications requiring high activity concentration.[30]

The results obtained with the proposed method were compared in all cases against the results obtained using only double coincidences (e.g., discarding all multiple events) and against the case in which triple coincidences are equally weighted among their possible LORs (average method). Finally, as the goal of this work is to show the effect on image quality and overall scanner performance of adding triple events to the standard coincidences, attenuation, scatter, and random corrections were not applied in any case.

2.D.1. Normalization correction for triple coincidences

To determine differences in scanner sensitivity for double and triple coincidences, we compared the axial and transaxial

profiles of the sinograms obtained for each type of event in the calibration procedure. The performance of the proposed normalization correction was evaluated by applying these corrections to sinograms of a uniformly filled cylinder containing either IDS or Rn_T coincidences. Images reconstructed using SSRB + FBP with a ramp filter were visually inspected for uniformity artifacts. To quantitatively determine which correction performed better, we calculated the percent standard deviation (standard deviation divided by the mean value) in a region of interest (ROI) of the reconstructed images containing 75% of the volume of the cylinder.

2.D.2. Scanner sensitivity

The relative sensitivity of the scanner for each type of event was obtained using a 6.8 μCi ^{18}F point source carefully centered in the transaxial direction of the FOV. Two-minute acquisitions were obtained while the source was being stepped in 0.75 mm increments across the scanner from end to end of the axial FOV. The activity was low enough so that dead time losses were negligible. At each acquisition point, a sinogram for each type of coincidence (doubles within a 400–700 keV energy window and Rn_T or IDS coincidences) was constructed (we used the average method to generate the IDS and Rn_T sinograms). Each sinogram was rebinned using SSRB and the total number of counts per slice was obtained. Slice sensitivity was calculated by dividing the total counts per slice by the activity present in the source after correcting for radioactive decay. It is important to highlight that the increase in sensitivity obtained by counting triple coincidences in this way is not giving any additional information other than the potential increase in sensitivity of the scanner. The amount of improvement or the effective increase in sensitivity will depend on the method used to assign the triple coincidences into LORs.

In this test, we also evaluated the number of triple events that would be processed as double coincidences in the scanner if no special treatment was used for triples. Those events would be all the Rn_T events (that would be included as two different LORs) and IDS events in which one of the IDS photons deposited energy above the lower energy threshold (400 keV).

2.D.3. Count-rate performance

The NEC rate is determined from the raw PET data (thus does not depend on factors such as normalization correction) and is used as an indicator of the image quality achievable by the system. Since several works demonstrated that the square of the image SNR is linearly related to the NEC rate for 3D acquisitions reconstructed using rebinned filtered backprojection,[31,32] this test allows one to evaluate the effect of adding triple coincidences as a function of the activity concentration and sample size. Scatter fraction and NEC-rate performance were measured using two cylindrical polyethylene phantoms[6,29] that simulated the dimensions of a mouse and a rat. Initial activity concentrations in the line source within each phantom were 54 and 6.8 μCi/cm³ for the mouse- and rat-sized

cylinders, respectively. Five-minute acquisitions were taken in list mode each hour over a 13-h period while the activity in the line source decayed. For each of the 5-min acquisitions, we applied the method described in the NEMA NU-4 protocol[29] to calculate true, prompt, random, and NEC rates, using standard sinograms just containing double coincidences or doubles plus triple events recovered using either the proportional method or the average method.

2.D.4. Image quality

To evaluate image quality, we used a NEMA NU-4 IQ phantom[29] which is composed of a main body that contains a fillable cylindrical chamber 30 mm in diameter and 30 mm in length and a solid part 20 mm in length into which 5 fillable rods with diameters of 1–5 mm have been drilled. A lid attached to the uniform region of the phantom supports two fillable compartments. These are hollow cylinders 15 mm in length and 8 mm in inner diameter with 1-mm wall thickness. The main compartment and the rods (Fig. 4) were filled with a 4 μCi/cm^3 ± 5% aqueous solution of ^{18}F. One of the two compartments was filled with water, while the other contained an activity concentration roughly four times the concentration used in the main compartment and fillable rods (16 μCi/cm^3 ± 5%). The phantom was scanned for 30 min in list mode and reconstructed using only double coincidences and doubles plus triple coincidences distributed using either the proportional or the average method.

Images from datasets with an increasing number of counts (doubles or doubles plus triple events) were generated to evaluate differences in image quality as a function of the acquisition time. The following ROIs were defined in the reconstructed images (Fig. 4).

- *Hot*: a 6 mm diameter by 7.5 mm length cylindrical region in the insert of the phantom with the highest activity concentration.
- *Cold*: a 6 mm diameter by 7.5 mm length cylindrical region in the insert of the phantom that was filled with nonradioactive water.
- *Background*: 22.5 mm diameter by 10 mm long cylindrical volume of interest over the center of the uniform region of the IQ phantom.
- *Rods*: 10 mm length cylindrical regions of interest with a diameter twice the physical diameter of each rod.
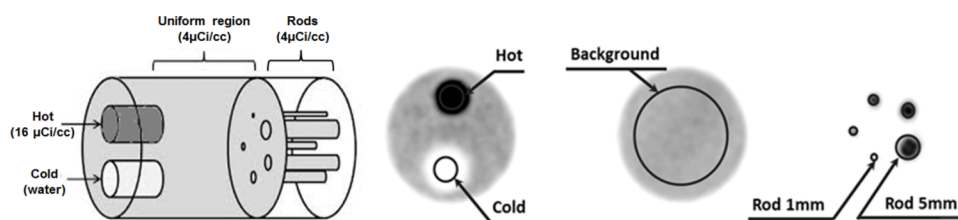
Quantitative figures of merit for SNR and contrast in the hot and cold ROIs were used in addition to the NEMA image-quality test. The SNR is a widely accepted metric that characterizes PET image quality because it reflects the relative signal level with respect to the noise of the reconstructed image and thereby is a metric related to lesion detectability.[33] The SNR of the hot and cold ROIs was computed using

$$\text{SNR} = \frac{|\mu_{\text{signal}} - \mu_{\text{bck}}|}{\sigma_{\text{bck}}}, \tag{5}$$

where μ_{signal} is the mean value in the ROI being evaluated and μ_{bck} is the mean value in the background ROI. The noise in the formula (σ_{bck}) is defined as the standard deviation of the pixel values in the background ROI. Since an increase in sensitivity implies the ability to acquire shorter scans with similar SNRs, we also evaluated if the increase in sensitivity due to the addition of triple coincidences enabled reductions in acquisition time.

Image contrast refers to differences in intensity in regions of the image with different levels of radioactive uptake and thus is indicative of the quantitative accuracy of the system. This parameter was evaluated in the hot and cold regions using the following expression:

$$\text{Contrast} = \frac{|\mu_{\text{signal}} - \mu_{\text{bck}}|}{\mu_{\text{bck}}}. \tag{6}$$

The standard deviation (%) in the background region, the percent spill-over ratio in the cold insert (mean value of the cold region divided by the mean value of the background region), and the contrast recovery coefficients, which are indicative of the spatial resolution of the system, were also evaluated using the images of the IQ phantom as indicated in the NEMA NU-4 protocol.[29]

2.D.5. Small-animal imaging

Finally, we evaluated the effect of adding triple coincidences to the standard PET data in a conventional small-animal imaging procedure. A 119-g rat was injected with 482 μCi of ^{18}F-FDG, and after a 40-min uptake period, the rat was scanned for 20 min (2 bed positions, 10 min/position). Images corresponding to different acquisition time points containing accumulated double coincidences (400–700 keV) or doubles plus triple coincidences recovered using our method

FIG. 4. A NEMA IQ phantom filled with ^{18}F was used to evaluate the effect of adding triple coincidences to the standard PET data. SNR and contrast were evaluated in the hot and cold regions of the phantom. The background ROI was used to estimate standard deviation (%) in the images and the rods were used to estimate the contrast recovery coefficients of the scanner. Rods are 5, 4, 3, 2, and 1 mm in diameter. ROIs in the rod regions had twice the physical diameter of each rod (not drawn to scale).
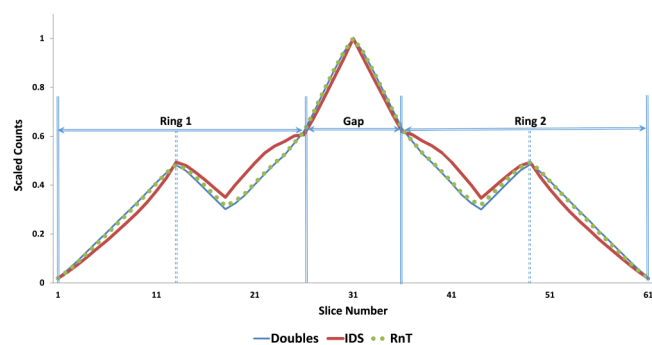
FIG. 5. Axial sensitivity profile for double and triple coincidences. Differences in the axial sensitivity profile of the scanner for double and triple events indicate the need to apply independent normalization corrections for some of the datasets. The profiles are scaled to the slice with the maximum number of counts for each type of event to allow their direct comparison. Vertical lines in the plot indicate the position of the center of the two rings of the scanner and the gap between them. Doubles: double coincidences, IDS: interdetector scattered events, Rn_T: random triple events.

were compared. In this case, images were reconstructed using SSRB, FBP, and a Butterworth filter (order 2, cutoff 0.4).

3. RESULTS

3.A. Normalization correction

Figure 5 shows the axial sensitivity profiles obtained for double, IDS, and Rn_T events. Sensitivity for IDS events in this scanner is increased for the LORs that have an interaction point close to the gaps between detector rings which, for most scanner configurations, represents a region with reduced sensitivity to standard coincidences. This can be clearly seen in the axial sensitivity profiles plotted in Fig. 5 in which an increased sensitivity to IDS coincidences is shown in the slices corresponding to the inner half of each detector ring (slices 13–26 and 34–47). This effect is attributable to IDS events scattering from one ring of detectors into the other.

Furthermore, differences among these profiles indicate that the standard normalization for double coincidences is not appropriate for normalization of IDS events. However, since the transaxial (not shown) and axial sensitivity profiles for Rn_T and double coincidences are similar, the same normalization correction might be used for both datasets. Additional evidence supporting this finding is shown in Fig. 6 in which
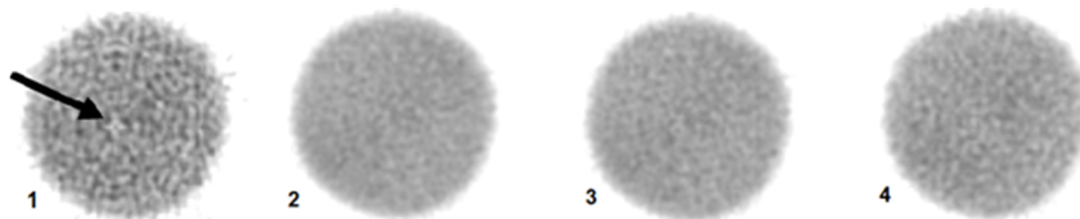
the effect of using mismatched normalization corrections can be appreciated in the reconstructed slices of a homogeneously filled cylindrical phantom. The uniformity artifacts visible in Fig. 6(1) indicate that the doubles normalization is not well-suited for correction of the IDS events. The remaining images [Fig. 6(2–4)] are artifact-free, showing that an appropriate normalization of IDS and Rn_T events is achieved with their respective specific calibrations. As the doubles correction still applies correctly for Rn_T events, and since it provides better statistics, this correction was used for Rn_T events in the experiments. Percent standard deviation measured in a ROI containing 75% of the volume of the phantom was of 36.3%, 16.2%, 17.1%, and 17.6% for the cases represented in Fig. 6 (1 to 4, respectively).

3.B. Scanner sensitivity

The apparent increase in sensitivity due to IDS and Rn_T events was 17.9% and 0.46%, respectively. Triple coincidences represented 95.4% of all the multiple coincidence events detected, and of those, 97.4% had two valid LORs (between allowed coincidence pairs of block detectors). Note that since the Rn_T event rate increases with the amount of activity and this test was performed at very low activity concentration, the potential increase in scanner sensitivity due to Rn_T events is not reflected in the results. Of the 17.9% IDS events detected during this test, only a 1.7% was events in which one of the IDS photons had energy above 400 keV, which means that most of these events would be effectively filtered by the energy window of current PET scanners in a standard acquisition.

3.C. Count-rate performance

The double-coincidences background in the scanner due to the intrinsic radioactivity of the detectors was found to be 6 counts/s for a 400–700 keV energy window. The triple coincidences background rate was not included in the calculations since it was found to be negligible (less than 0.25 counts/s for IDS events and ~0 counts/s for Rn_T events). Figure 7 (left) shows the NEC curves obtained for each phantom (mouse and rat) and combination of events (doubles, doubles + IDS, and doubles + IDS + Rn_T) when the proposed methodology for recovery of triple coincidences was used. The contribution of

FIG. 6. Effect of normalization correction. Images 1–4 are FBP-reconstructed slices of a cylindrical phantom uniformly filled with ^{18}F. Images 1 and 2 were obtained after applying the normalization correction for doubles and for IDS events, respectively, to a sinogram containing only IDS recovered events. Images 3 and 4 were obtained after applying the doubles normalization correction and the Rn_T matched correction, respectively, to a sinogram containing only Rn_T recovered events. Uniformity artifacts, clearly visible in (1), are caused by mismatched scanner sensitivity between double and IDS coincidences. Images 2–4 are properly corrected and artifact-free. In all the cases, triple coincidences were recovered using the proportional method.
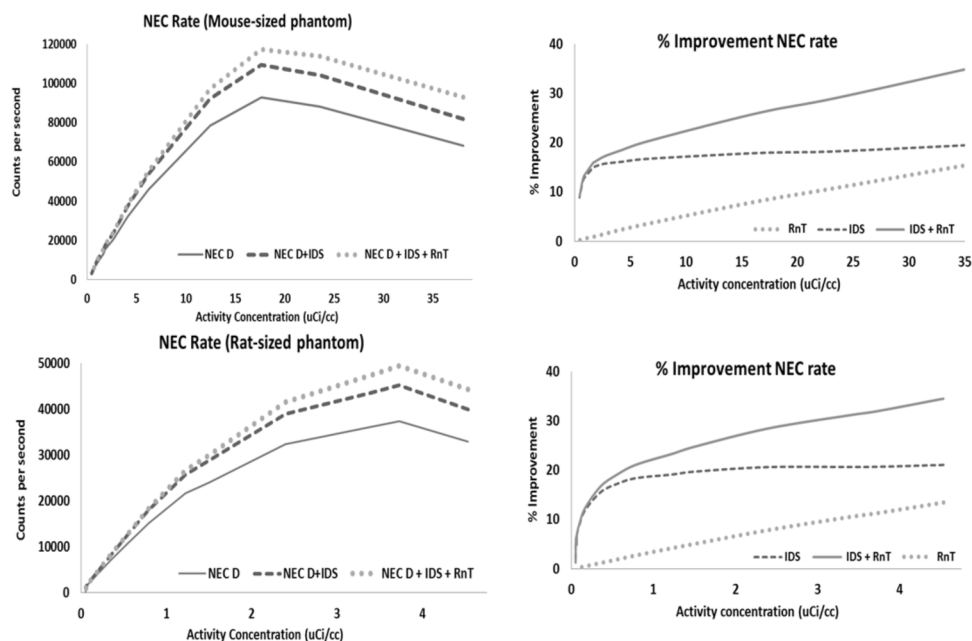
FIG. 7. Noise-equivalent count rates obtained for mouse- and rat-sized phantoms (left) and percentage improvement in NEC rates due to the addition of triple events as a function of the activity concentration (right). Peak NEC rates for double coincidences and double plus triple-coincidence events are shown in (Table I) for both phantoms and recovery methods. Triple-coincidence data used to generate these plots were recovered using the proposed method.

IDS events to the NEC is almost constant and does not depend on the activity concentration or object size. On the other hand, since the Rn_T event rate increases with the activity in the FOV, the relative contribution of these events is a function of this parameter and is also related to the object size [Fig. 7 (right)]. In this study, random triple events coming from three different annihilations were considered negligible compared to Rn_T. In any case, it would be possible to estimate the relative abundance of these events using a delayed time window for triples and thus calculate a correction for the triples dataset.

In general terms, the contribution of triple events recovered using our method to the NEC curve increases with the doubles NEC rate until the peak is achieved and remains almost constant from there. This behavior is related to several factors: first, the higher the doubles NEC rate, the better the SNR in the doubles histogram used as a "reference" by the recovery method, and therefore, the performance of the method is expected to be higher. Second, if there is no information in the "doubles" histogram ($D_{i-j} = D_{i-k} = 0$ or $D_{i-j} = D_{j-k} = 0$) related to the triple interaction being evaluated, the triple event will be discarded avoiding the inclusion of extra noise in the resulting triples histogram. At the activity concentration

values where the peak rates were reached (Table I), the relative contribution of IDS and Rn_T events recovered using the proportional method incremented NEC values by 26.6% and 32% for mouse- and rat-sized objects, respectively, while the average method resulted in almost no improvement for the rat-sized phantom and a mild improvement (7.6%) for the mouse-sized phantom. Furthermore, the proposed method reduced the apparent SF (ratio between scattered events and true events) in the data in both cases (7.7% for mouse and 2.75% for the rat phantom) while the average method increased this fraction by 30.4% and 17.8% for the mouse- and rat-sized objects, respectively. Since the total scatter fraction is reduced when triple events recovered with the proportional method were added to the double coincidences, the fraction of triple events classified as true events must be greater than that fraction for double coincidences. Note that the activity concentration in the phantoms during these measurements was very low, and consequently, the total number of counts in the sinograms used to calculate the SF was small too, with several bins with zero value and with most of the counts concentrated in the bins corresponding to the line insert of the phantoms. In this situation, the algorithm provides much higher weights to those

TABLE I. Counting rate performance of the Argus scanner. Peak NEC rates in k counts/s.

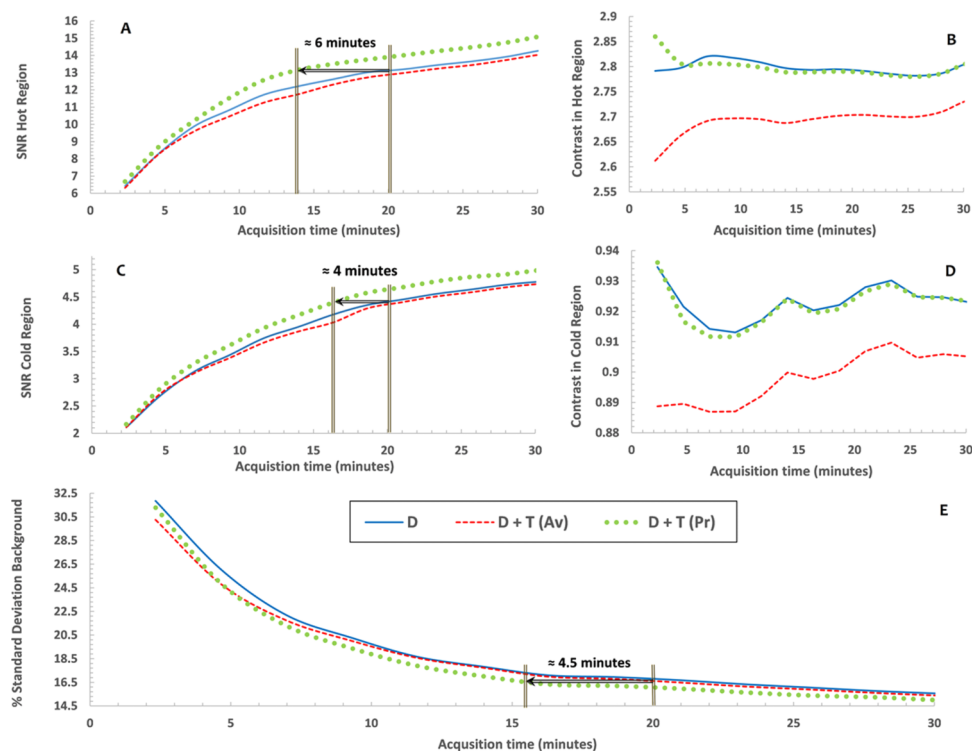|		Rat (3.72 μCi/cm^3)		Mouse (17.6 μCi/cm^3)	
		Peak NEC	SF (% ± SD)	Peak NEC	SF (% ± SD)
	D	37.39	23.28 ± 1.16	92.82	13.75 ± 0.55
Average method	D + IDS	37.54	26.90 ± 1.05	96.73	17.77 ± 0.56
	D + IDS + Rn_T	37.91	27.42 ± 1.11	99.83	17.93 ± 0.58
Proportional method	D + IDS	45.12	22.65 ± 1.18	109.59	12.73 ± 0.57
	D + IDS + Rn_T	49.34	22.64 ± 1.19	117.52	12.69 ± 0.59

FIG. 8. SNR and contrast in the hot [(A) and (B)] and cold [(C) and (D)] ROIs and standard deviation (%) in the background ROI (E) for double and for double + triple events as a function of the acquisition time. Triple events were recovered using either the proportional method $[D+T(\mathrm{Pr})]$ or the averages method $[D+T(\mathrm{Av})]$. Assuming a target acquisition time of 20-min, the use of triple coincidences produced similar levels of SNR and percentage noise in ~80% of the acquisition time.

lines passing through the line insert and discards most of the lines not crossing the line source, which in turn explains the improvement in the observed SF.

Finally and again due to the low activity concentration in the phantoms during the SF measurement,[29] the relative contribution of Rn_T events to this parameter is not reflected in the results shown in Table I (i.e., the Rn_T rate was negligible).

3.D. Image quality

3.D.1. Signal-to-noise ratio and standard deviation

Figure 8 shows the SNR in the cold and hot ROIs of the IQ phantom, as well as standard deviation (%) in the background ROI. The plot was generated using datasets with an increasing number of double or double plus triple events recovered using either the average or the proportional method. The proposed proportional method consistently produced images with reduced standard deviation (%) and higher SNR, while the average method slightly reduced the standard deviation (%) in the uniform region of the phantom but provided worse SNR in

the hot and cold ROIs than that achieved by discarding all the triples. Note that image degradation obtained with the average method is also caused by the use of the doubles normalization correction for IDS events. Even though from the results shown in Sec. 3.A it is clear that a specific normalization correction would also be necessary in this case, we preferred not to use this specific correction to better compare our approach with state-of-the-art methodologies.

Using data acquired for 20 min (the NEMA protocol specifies a 20-min acquisition for the image-quality test[29]), absolute improvements in SNR due to the recovery of triple coincidences with our method were 5.36% and 4.5% in the hot and cold regions, respectively, while reduction in standard deviation (%) in the uniform region was 4.94%. Although improvements in SNR are relatively small in magnitude, they are large enough to allow a significant reduction in acquisition time for a given SNR level. As shown in Fig. 8, and again using as a reference the 20-min acquisition time defined in the NEMA protocol, the use of triple coincidences allows obtaining similar levels of SNR and standard deviation (%) as those obtained

TABLE II. Contrast in the hot and cold regions and percentage SOR in the cold region [± standard deviation (%)] [standard deviation (%) was calculated from images at different acquisition time points (Fig. 8)].

		Hot	Cold	%SOR
	Doubles	2.79% ± 0.48%	0.91% ± 0.74%	10.21% ± 5.87%
Average method	$D + \mathrm{IDS} + \mathrm{Rn}_T$	2.71% ± 1.25%	0.89% ± 0.86%	11.91% ± 7.05%
Proportional method	$D + \mathrm{IDS} + \mathrm{Rn}_T$	2.78% ± 0.52%	0.91% ± 0.81%	10.52% ± 6.01%

TABLE III. Contrast recovery coefficients ± standard deviation (%) [standard deviation (%) was calculated as defined in the NEMA NU4 protocol (Ref. 29)].

		1 mm	2 mm	3 mm	4 mm	5 mm
	Doubles	0.28% ± 31.0%	0.54% ± 23.4%	0.79% ± 23.5%	0.96% ± 22.5%	1.10% ± 22.7%
Average method	D + IDS + Rn_T	0.27% ± 30.3%	0.52% ± 22.9%	0.75% ± 23.6%	0.93% ± 22.4%	1.07% ± 22.4%
Proportional method	D + IDS + Rn_T	0.28% ± 30.5%	0.54% ± 23.0%	0.79% ± 22.5%	0.96% ± 21.5%	1.11% ± 21.7%

using only double coincidences in ∼80% of the acquisition time [the SNR in the cold region (Fig. 8) was used to provide this estimation]. Importantly, it can be seen in Fig. 8 that the reduction in acquisition time provided by this method depends on our target SNR. For example, if our target SNR is that achieved after a 10-min acquisition time using only double coincidences, the relative reduction in acquisition time provided by the use of triples is ∼13%, instead of the ∼20%, obtained when the target is the SNR resulting from a 20-min acquisition time. In addition, it is also important to note that the NEMA protocol states that the main compartment of the phantom has to be filled with 100 μCi, which is a very low activity concentration, even for mouse imaging (i.e., people generally use 250–500 μCi). At higher values of activity concentration, the increased number of Rn_T events combined with better statistics in the doubles dataset may serve to provide better improvements from the addition of triple coincidences (see Sec. 3.D.3).

3.D.2. Contrast, percentage SOR, and recovery coefficients

The results in Table II show contrast values obtained in the hot and cold regions using either doubles or doubles plus triple events after a 20-min acquisition. In the cold region, since no activity was present, ideally a contrast of 1 should be obtained from Eq. (6). Similarly, since the activity in the hot region was four times the activity concentration in the background region (Fig. 4), a contrast equal to 3 would be obtained for that ROI. The values presented in the table were achieved with a relatively small number of counts for images containing either double or double plus triple coincidences. Variations of

contrast in both regions as a function of the number of counts included in the plots (Fig. 8) were not significant (e.g., the standard deviation (%) values in Table II). This implies that if triple coincidences are used to reduce acquisition time, not only the SNR but also the contrast will be similar to that obtained using standard coincidences and a longer acquisition time. Contrast was consistently worsened in both ROIs when the average method was used to recover triple coincidences.

Percentage spill-over ratio in final images (20-min acquisition) was found to be worsened by 3.1% and by 16.7% when adding triple coincidences to the standard double-coincidences dataset with our method and with the average method, respectively (Table II). Spill-over ratios are commonly used to assess the performance of the scatter and random correction algorithms; however, those corrections were not applied to the double-coincidences datasets used in the present study. As indicated in Sec. 2.C, such corrections can be applied to the doubles dataset before its use in the proposed recovery method. The use of a corrected version of the doubles dataset, although not addressed in this work, could provide not only improvements in this figure of merit (percentage SOR) but also an overall increase in performance, since the activity distribution used to sort triple coincidences will be more accurate. The proposed method also provided CRC values similar to those obtained with double coincidences (Table III) while also reducing the standard deviation due to the addition of extra counts. In contrast, the average method worsened the contrast recovery coefficients of the system, even though it provided a reduction of SD (%) in two of the five spheres.
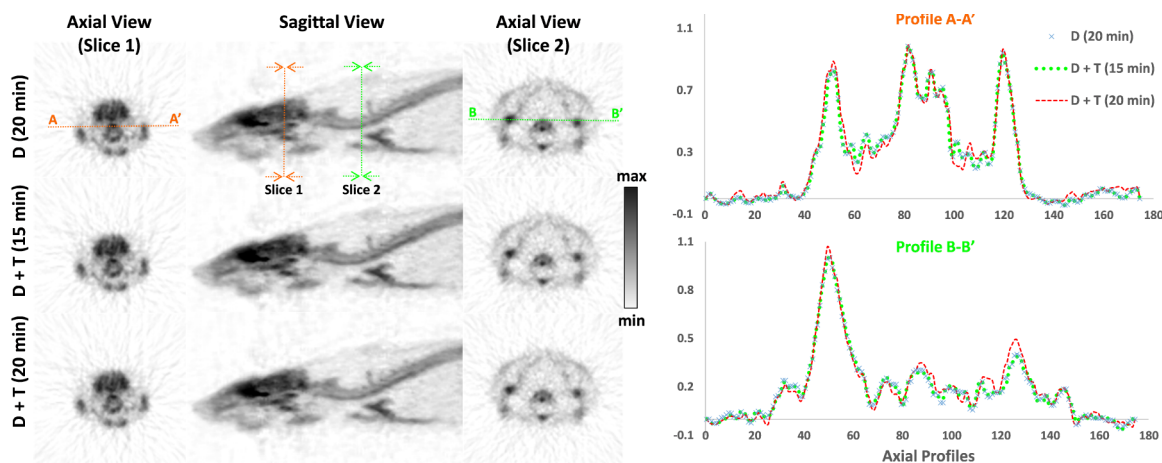

FIG. 9. Sagittal and axial views of a rat injected with ^{18}F-FDG. Images shown were obtained using all double coincidences and double plus triple coincidences recorded during ∼75% and 100% of the acquisition time (20 min). Shown on the right are profiles (A – A′ and B – B′) along the axial views (slice 1 and 2) comparing the results obtained in each case.

3.D.3. Small-animal imaging

The ^{18}F-FDG dose injected into the animal ($\sim$4 μCi/cm^3) was chosen to maximize the NEC-rate performance of the scanner and thus the amount of improvement provided by the inclusion of triple coincidences (see Sec. 3.C). Figure 9 shows sagittal views of the rat along with axial slices corresponding to positions denoted as slice 1 and slice 2. The plots on the right are profiles along the axial views (A - A′ and B - B′) comparing the values for double events (400–700 keV) accumulated during the 20-min acquisition with those obtained after adding double and triple coincidences using only the first 15.1 min of the acquisition and the 20-min acquisition. As can be seen, similar levels of SNR were found in the 15.1 (doubles plus triples) and 20 min (doubles only) images demonstrating that a reduction of acquisition time on the order of ∼25% can be achieved in this standard imaging procedure. Moreover, a direct comparison between the 20-min images containing either double or double plus triples shows an increase in SNR due to the effective increase in sensitivity, consistent with the results obtained in the NEC-rate measurements.

4. DISCUSSION AND CONCLUSIONS

While previous attempts to increase the sensitivity of PET scanners using IDS events have been focused on systems using specialized detectors,[12,13,21–23] this work demonstrates that those events can not only be detected but also effectively used in conventional block-detector-based scanners. Moreover, since our method only uses the distribution of standard PET coincidences to estimate the most probable distribution for IDS events, it does not suffer from limitations imposed by the energy resolution of the detectors as occurs with Compton-scatter kinematics-based methods. In addition, this approach allows the recovery of other types of significant triple coincidences, such as Rn$_T$, which could not be recovered by any method based on Compton kinematics. Furthermore, although we only used ^{18}F in this work, our proposed method can also be directly applied to the triple coincidences of positron-gamma emitter PET radionuclides.

This work demonstrates that normalization correction is a key factor for using the information contained in IDS events effectively. To our knowledge, only a contemporary study[24] took into account the possibility of having different sensitivity profiles for double and IDS coincidences, while in previous works, standard normalizations were applied to datasets containing double and IDS events.[12,13] Importantly, adding incorrectly normalized data to the standard PET coincidences can adversely affect image-quality metrics such as SNR or contrast-to-noise ratio, which may further explain results found in the earlier studies[13] that utilized real data from a scanner. In this work, we provide a general method to generate normalization correction for triple coincidences which is effective and can be obtained from the same acquisition used for calibration of double coincidences. However, it would require a longer acquisition time than the one used for double coincidences, or the use of some appropriate noise-reduction

strategy,[28] in order to obtain similar statistical precision for double and triple coincidences.

Although the proposed methodology can be incorporated within a state-of-the-art 3D iterative reconstruction algorithm, we preferred to use a standard FBP reconstruction because image quality provided by iterative algorithms not only depends on the statistical properties of the data but also on their specific implementation, the accuracy of the system model, and the number of iterations among other elements. An important factor that should be considered when implementing the proposed method within an iterative reconstruction algorithm is that since our method adds noninteger values to the data, datasets containing double and triple coincidences will not be "by definition" Poisson distributed. Although most iterative reconstruction algorithms for PET assume Poisson statistics, it is possible to derive common reconstruction algorithms such as OSEM without assuming this distribution.[34]

In the Argus scanner, IDS events provided an almost constant increment of ∼18% in the true-event rate which does not depend on the distribution of the activity, whereas the increase provided by Rn$_T$ events is a function of this parameter and ranged from ∼0.1% with low activity to more than 8% at the activity concentrations where peak NEC rates were achieved [Fig. 7 (right)]. This increase in sensitivity translated into improvements of 26.6% and 32% in peak NEC rates for mouse- and rat-sized objects, respectively. The amount of improvement provided by the inclusion of triple events has been shown to increase with both the doubles NEC rate and the absolute rate of triple coincidences. These results were consistent with those obtained in the image-quality experiments, for which we found that bigger reductions in acquisition time were achievable when higher levels of image SNR were the target (Fig. 8). In fact, both findings are related to the number of counts recorded in the doubles histogram or, in other words, the amount of noise in the dataset used as a reference by the proportional method. Since for Poisson distributed variables, the relative standard deviation of the measurement (e.g., in each bin of a sinogram) is related to the inverse square-root of the number of counts recorded (in the corresponding bin), it is logical to expect that a doubles histogram with a higher count density will provide smaller uncertainties for the distribution of triple coincidences and, consequently, a better improvement in the SNR of the final image. This may be a big advantage in clinical scanners, since those systems use sinogram bin sizes much bigger than those used in preclinical scanners, and thus, a higher count density can be expected in the doubles dataset.

Regarding practical considerations for the implementation of this method in other scanners (i.e., clinical scanners), it must be taken into account that to recover IDS events, it is necessary to broaden the hardware energy acceptance window, and this can increase the dead time and affect the counting capabilities of the system (e.g., NEC rates), since we will be recording many more events than with a narrow energy window centered at 511 keV. In our case, since the hardware energy-acceptance window of the scanner is set by default to 90–750 keV (the energy windowing is done by software) and we changed it to 50–800 keV, this effect was negligible. However, if the

acquisition electronics of the target scanner are not adequate for working in this mode, the extra dead time due to the increased number of events recorded can negatively affect the scanner performance. Fortunately, acquisition electronics for PET systems have evolved from analog implementations to highly parallelized digital systems using free-running analog-to-digital converters which introduce almost negligible dead time,[32,33] thus mitigating this potential flaw in performance. Another interesting consideration in clinical scanners is that the time-of-flight (TOF) capabilities of those systems can be easily combined with the proposed algorithm, for example, by using a methodology similar to that proposed in Ref. 7 to assign timestamps to each LOR in a triple event.

The proposed method to recover triple coincidences combined with appropriate normalization corrections has been shown to be capable of providing images with SNR superior to that achievable by using only standard coincidences, while preserving contrast (does not introduce bias) and spatial resolution. Similarly, the increased sensitivity provided by triple coincidences can be effectively used to reduce the acquisition time required to obtain a given SNR in the images. As we showed in Sec. 3.D, inclusion of triple events allowed us to achieve levels of SNR in a NEMA image-quality test similar to those achieved using only double coincidences in ~80% of the time. More importantly, when adjusting injected dose values based on NEC performance of the scanner, the use of triple coincidences allowed us to achieve a ~25% reduction in acquisition time (Fig. 9) during a common preclinical PET imaging protocol.

ACKNOWLEDGMENTS

[a] Author to whom correspondence should be addressed. Electronic mail: elage@mit.edu

[1] R. Nutt, "Is LSO the future of PET?," Eur. J. Nucl. Med. Mol. Imaging **29**, 1523–1525 (2002).

[2] G. Borasi *et al.*, "PET systems: The value of added length," Eur. J. Nucl. Med. Mol. Imaging **37**, 1629–1632 (2010).

[3] B. J. Kemp *et al.*, "NEMA NU 2-2001 performance measurements of an LYSO-based PET/CT system in 2D and 3D acquisition modes," J. Nucl. Med. **47**, 1960–1967 (2006), see http://www.ncbi.nlm.nih.gov/pubmed/17138738.

[4] S. Surti *et al.*, "Performance of philips gemini TF PET/CT scanner with special consideration for its time-of-flight imaging capabilities," J. Nucl. Med. **48**, 471–480 (2007), http://www.ncbi.nlm.nih.gov/pubmed/17332626.

[5] B. W. Jakoby *et al.*, "Physical and clinical performance of the mCT time-of-flight PET/CT scanner," Phys. Med. Biol. **56**, 2375–2389 (2011).

[6] A. L. Goertzen *et al.*, "NEMA NU 4-2008 comparison of preclinical PET imaging systems," J. Nucl. Med. **53**, 1300–1309 (2012).

[7] A. A. Wagadarikar *et al.*, "Sensitivity improvement of time-of-flight (TOF)-PET detector through recovery of Compton scattered annihilation photons," in *2012 IEEE Nuclear Science Symposium and Medical Imaging Conference (NSS/MIC)* (IEEE, 2012).

[8] J. Cal-González *et al.*, "Simulation of triple coincidences in PET," Phys. Med. Biol. **60**, 117–136 (2015).

[9] D. P. McElroy *et al.*, "Characterization and readout of MADPET-II detector modules: Validation of a unique design concept for high resolution small animal PET," IEEE Trans. Nucl. Sci. **52**, 199–204 (2005).

[10] M. Bergeron *et al.*, "Performance evaluation of the LabPET APD-based digital PET scanner," IEEE Trans. Nucl. Sci. **56**, 10–16 (2009).

[11] R. Prasad *et al.*, "NEMA NU-04-based performance characteristics of the LabPET-8™ small animal PET scanner," Phys. Med. Biol. **56**, 6649–6664 (2011).

[12] M. Rafecas *et al.*, "Inter-crystal scatter in a dual layer, high resolution LSO-APD positron emission tomography," Phys. Med. Biol. **48**, 821–848 (2003).

[13] J. Clerk-Lamalice *et al.*, "Evaluation of easily implementable Inter-Crystal scatter recovery schemes in high-resolution PET imaging," in *IEEE Nuclear Science Symposium and Medical Imaging Conference Record (NSS/MIC), Anaheim, CA* (IEEE, 2012), Vol. 2013.

[14] M. Lubberink and H. Herzog, "Quantitative imaging of 124I and 86Y with PET," Eur. J. Nucl. Med. Mol. Imaging **38**, 10–18 (2011).

[15] H. Lin, K. Chuang, S. Chen, C. Chiang, C. Lin, and M. Jan, "Recycling of triple coincidences for nonpure positron emitters in MiroPET imaging," Eur. J. Nucl. Med. Mol. Imaging **39**, S155–S303 (2012).

[16] K. Kacperski and N. M. Spyrou, "Performance of three-photon PET imaging: Monte Carlo simulations," Phys. Med. Biol. **50**, 5679–5695 (2005).

[17] K. Mercurio *et al.*, "The three-photon yield from e+ annihilation in various fluids," Phys. Med. Biol. **51**, N323–N329 (2006).

[18] S. Surti *et al.*, "Correction technique for cascade gammas in I-124 imaging on a fully-3D, time-of-flight PET scanner," IEEE Trans. Nucl. Sci. **56**, 653–660 (2009).

[19] K. A. Comanor *et al.*, "Algorithms to identify detector Compton scatter in PET modules," IEEE Trans. Nucl. Sci. **43**, 2213–2218 (1996).

[20] A. Braem *et al.*, "Feasibility of a novel design of high resolution parallax-free Compton enhanced PET scanner dedicated to brain research," Phys. Med. Biol. **49**, 2547–2562 (2004).

[21] G. Pratx and C. S. Levin, "Bayesian reconstruction of photon interaction sequences for high-resolution PET detectors," Phys. Med. Biol. **54**, 5073–5094 (2009).

[22] Y. Gu *et al.*, "Effects of multiple-interaction photon events in a high-resolution PET system that uses 3-D positioning detectors," Med. Phys. **37**, 5494–5508 (2010).

[23] G. Chinn and C. S. Levin, "A maximum NEC criterion for Compton collimation to accurately identify true coincidences in PET," IEEE Trans. Med. Imaging **30**, 1341–1352 (2011).

[24] J. E. Gillam *et al.*, "Sensitivity recovery for the AX-PET prototype using inter-crystal scattering events," Phys. Med. Biol. **59**, 4065–4083 (2014).

[25] Y. Wang *et al.*, "Performance evaluation of the GE healthcare eXplore VISTA dual-ring small-animal PET scanner," J. Nucl. Med. **47**, 1891–1900 (2006), see http://www.ncbi.nlm.nih.gov/pubmed/17079824.

[26] J. J. Vaquero *et al.*, "Effects of the super bialkali photocathode on the performance characteristics of a position-sensitive depth-of-interaction PET detector module," IEEE Trans. Nucl. Sci. **57**, 2437–2441 (2010).

[27] R. D. Badawi *et al.*, "Algorithms for calculating detector efficiency normalization coefficients for true coincidences in 3D PET," Phys. Med. Biol. **43**, 189–205 (1998).

[28] M. Defrise *et al.*, "A normalization technique for 3D PET data," Phys. Med. Biol. **36**, 939–952 (1991).

[29] NEMA NU-4 *Performance Measurements for Small Animal Positron Emission Tomographs* (National Electrical Manufacturers Association, Rosslyn, VA, 2008).

[30] T. Chang *et al.*, "Reliability of predicting image signal-to-noise ratio using noise equivalent count rate in PET imaging," Med. Phys. **39**, 5891–5900 (2012).

[31] S. C. Strother *et al.*, "Measuring PET scanner sensitivity: Relating count rates to image signal-to-noise ratios using noise equivalents counts," IEEE Trans. Nucl. Sci. **37**, 783–788 (1990).

[32] C. C. Watson, "Count rate dependence of local signal-to-noise ratio in positron emission tomography," IEEE Trans. Nucl. Sci. **51**, 2670–2680 (2004).

[33] T. H. Farquhar *et al.*, "ROC and LROC analyses of the effects of lesion contrast, size, and signal-to-noise ratio on detectability in PET images," J. Nucl. Med. Off. Publ. Soc. Nucl. Med. **41**, 745–754 (2000), see http://www.ncbi.nlm.nih.gov/pubmed/10768578.

[34] M. E. Daube-Witherspoon *et al.*, "An iterative image space reconstruction algorithm suitable for volume ECT," IEEE Trans. Med. Imaging **5**, 61–66 (1986).